0026-895X/10/7804-600–607$20.00
MOLECULAR PHARMACOLOGY
Vol. 78, No. 4
65458/3625812
Mol Pharmacol 78:600–607, 2010
Printed in U.S.A.

Phenylalanine-544 Plays a Key Role in Substrate and Inhibitor Binding by Providing a Hydrophobic Packing Point at the Active Site of Insulin-Regulated Aminopeptidase[S]

Anthony L. Albiston, Vi Pham, Siying Ye, Leelee Ng, Rebecca A. Lew, Philip E. Thompson, Jessica K. Holien, Craig J. Morton, Michael W. Parker, and Siew Yeen Chai

Howard Florey Institute, Florey Neurosciences Institutes (V.P., S.Y., L.N., S.Y.C., A.L.A.), Centre for Neuroscience (S.Y.C.), and Department of Biochemistry and Molecular Biology, Bio21 Molecular Science and Biotechnology Institute (M.W.P.), University of Melbourne, Parkville, Victoria, Australia; Department of Biochemistry & Molecular Biology, Monash University, Clayton, Victoria, Australia (R.A.L.); Medicinal Chemistry and Drug Action, Monash Institute of Pharmaceutical Sciences, Parkville, Victoria, Australia (P.E.T.); and St. Vincent's Institute of Medical Research, Fitzroy, Victoria, Australia (J.K.H., C.J.M., M.W.P.)

Received April 7, 2010; accepted July 2, 2010

ABSTRACT

Inhibitors of insulin-regulated aminopeptidase (IRAP) improve memory and are being developed as a novel treatment for memory loss. In this study, the binding of a class of these inhibitors to human IRAP was investigated using molecular docking and site-directed mutagenesis. Four benzopyran-based IRAP inhibitors with different affinities were docked into a homology model of the catalytic site of IRAP. Two 4-pyridinyl derivatives orient with the benzopyran oxygen interacting with the Zn^{2+} ion and a direct parallel ring-stack interaction between the benzopyran rings and Phe544. In contrast, the two 4-quinolinyl derivatives orient in a different manner, interacting with the Zn^{2+} ion via the quinoline nitrogen, and Phe544 contributes an edge-face hydrophobic stacking point with the benzopyran moiety. Mutagenic replacement of Phe544 with alanine, isoleucine, or valine resulted in either complete loss of catalytic activity or altered hydrolysis velocity that was substrate-dependent. Phe544 is also important for inhibitor binding, because these mutations altered the K_i in some cases, and docking of the inhibitors into the corresponding Phe544 mutant models revealed how the interaction might be disturbed. These findings demonstrate a key role of Phe544 in the binding of the benzopyran IRAP inhibitors and for optimal positioning of enzyme substrates during catalysis.

Introduction

Insulin-regulated aminopeptidase (IRAP; E.C. 3.4.11.3) is a 165-kDa type II membrane-bound glycoprotein belonging to the M1 family of zinc metallopeptidases (Albiston et al., 2004b). The catalytic activity of IRAP has been characterized in vitro, with vasopressin, oxytocin, leu-enkephalin, bradykinin, and somatostatin identified as substrates (Herbst et al., 1997; Lew et al., 2003). Two recent reports have indicated a role for IRAP in the processing of antigenic peptides for major histocompatibility complex class 1 cross-presentation (Saveanu et al., 2009; Segura et al., 2009). This indicates broad substrate specificity, although the main identified substrates for IRAP contain either a tyrosine or phenylalanine at or near the amino terminus of the peptide. Pharmacological inhibition of IRAP in the brain improves memory in normal rodents (Lee et al., 2004; Albiston et al., 2008) and in animals with memory deficits induced by a range of perturbations (Wisniewski et al., 1993; Krishnan et al., 1999), including

This research was supported by the Robert J. Kleberg Jr. and Helen C. Kleberg Foundation; the Alzheimer's Drug Discovery Foundation; a Neurosciences Victoria/Victorian State Government Science, Technology, and Innovation Grant; the National Health and Medical Research Council (NHMRC) [Development Grants 454714 and 520695]; an NHMRC Peter Doherty fellowship (to V.P.); an Australian Research Council Federation Fellowship (to M.W.P.); an NHMRC Honorary Fellowship (to M.W.P.); and an NHMRC Senior Research Fellowship (to S.Y.C.).

A.L.A and V.P. contributed equally to this work

Article, publication date, and citation information can be found at http://molpharm.aspetjournals.org.
doi:10.1124/mol.110.065458.

[S] The online version of this article (available at http://molpharm.aspetjournals.org) contains supplemental material.

ABBREVIATIONS: IRAP, insulin-regulated aminopeptidase; APN, aminopeptidase N; Ang IV, angiotensin IV; AVP, arginine[8] vasopressin; HEK, human embryonic kidney; HFI, Howard Florey Institute; HFI-142, ethyl 2-amino-7-hydroxy-4-pyridin-3-yl-4H-chromene-3-carboxylate; HFI-419, ethyl 2-acetylamino-7-hydroxy-4-pyridin-3-yl-4H-chromene-3-carboxylate; HFI-435, ethyl 2-amino-7-hydroxy-4-quinolin-3-yl-4H-chromene-3-carboxylate; HFI-437, ethyl 2-acetylamino-7-hydroxy-4-quinolin-3-yl-4H-chromene-3-carboxylate; Leu-MCA, L-leucine-4-methyl-7-coumarinylamide; Leu-Enk, leu-enkephalin; LTA4H, leukotriene A4 hydrolase; LVV-H7, Leu-Val-Val-hemorphin-7; MCA, 7-amino-4-methylcoumarin; TFA, trifluoroacetic acid.

chemical disruption of the septohippocampal cholinergic pathway (Pederson et al., 1998, 2001; Albiston et al., 2004a; Olson et al., 2004). More recently, inhibition of aminopeptidase activity of IRAP in the brain has been linked to anticonvulsant properties (Stragier et al., 2006). There are currently two classes of IRAP inhibitors: peptide-based inhibitors (Lew et al., 2003) and the recently identified benzopyran-based series of inhibitors (Albiston et al., 2008).

Two distinct peptide inhibitors of IRAP have been identified: angiotensin IV (Ang IV) and Leu-Val-Val-hemorphin-7 (LVV-H7), both competitive inhibitors of IRAP that bind to the catalytic site with nanomolar affinities (Lew et al., 2003). Peptidomimetic approaches have developed further inhibitors of the enzyme (Axén et al., 2007; Andersson et al., 2008; Lukaszuk et al., 2008, 2009), predominantly Ang IV analogs with increased stability, but without significant improvement in affinity for IRAP. A tyrosine near the N terminus of the peptide inhibitors is a key amino acid residue for both Ang IV (Tyr^2) and LVV-H7 (Tyr^4); alanine substitution of this amino acid results in complete loss of binding to IRAP (Sardinia et al., 1993; Lee et al., 2003). Specificity is an issue with these peptide inhibitors of IRAP because they are able to bind to aminopeptidase N (APN) and the G-protein-coupled receptors, in addition to angiotensin AT_1 and the μ opioid receptors, at micromolar concentration (Demaegdt et al., 2006).

The second series consists of small-molecule benzopyran-based inhibitors [Howard Florey Institute (HFI) series] with nanomolar affinities for IRAP (Albiston et al., 2008). These were identified using a virtual screening approach against a homology model of the catalytic domain of IRAP and a subsequent medicinal chemistry campaign. The most potent inhibitors found to date include either a 4-(pyridin-3yl) or a 4-(isoquinolin-3-yl) substituent at the benzopyran and also a 2-amino or 2-acetamido substitution (Fig. 1) (Albiston et al., 2008). Although first identified by virtual screening, no biochemical evidence was available to characterize the molecular basis of inhibition, which is an important objective for the advancement toward a therapeutic candidate. The aim of the current study was to investigate the interactions of the inhibitors with the catalytic site of human IRAP by combining mutagenesis-based biochemical and in silico approaches. We designed mutagens around Phe544 of IRAP by successively reducing the size of the side chain but maintaining the hydrophobic nature of the site. We have investigated the effect of these mutations upon the inhibitor affinity, theoretical binding poses, and the hydrolysis of multiple IRAP substrates.

Materials and Methods

Materials. Ang IV, Nle^1-Ang IV, LVV-H7, (Arg^8)-vasopressin (AVP), and leu-enkephalin (Leu-Enk) were purchased from Auspep (Melbourne, VIC, Australia). The fluorescent substrate L-leucine-4-methyl-7-coumarinylamide (Leu-MCA), its cleavage product 7-amino-4-methylcoumarin (MCA), and all other reagents were purchased from Sigma (Castle Hill, NSW, Australia). HFI-142 (ethyl 2-amino-7-hydroxy-4-pyridin-3-yl-4*H*-chromene-3-carboxylate), HFI-419 (ethyl 2-acetylamino-7-hydroxy-4-pyridin-3-yl-4*H*-chromene-3-carboxylate), HFI-435 (ethyl 2-amino-7-hydroxy-4-quinolin-3-yl-4*H*-chromene-3-carboxylate) and HFI-437 (ethyl 2-acetylamino-7-hydroxy-4-quinolin-3-yl-4*H*-chromene-3-carboxylate) were synthesized by Epichem (Perth, SA, Australia) according to methods described previously (Albiston et al., 2008).

Molecular Modeling of the Catalytic site of IRAP. The protease domain of human IRAP (residues Leu140 to Ser533) was modeled on the structure of the equivalent domain of leukotriene A4 hydrolase (E.C. 3.3.2.6; LTA4H), (residues Ser8 to Leu389, Protein Data Bank code 1HS6) (Thunnissen et al., 2001). Although the overall identity between the sequences is low, the region immediately surrounding the active site residues, including the HEXXH and GXMEN motifs, is relatively well conserved, with 41% sequence identity. A sequence alignment of the catalytic domains of several different members of the M1 aminopeptidase family, including IRAP and LTA4H, was used to guide model building (data not shown). The model was built using COMPOSER in Sybyl6.8 (Tripos Inc., St Louis, MO) and minimized in Sybyl6.8 under the Tripos forcefield, the final structure having more than 95% of residues in the allowed region of a Ramachandran plot. Zinc was manually added to the active site motif after comparison with the zinc-bound LTA4H structure indicated the conformation of residues in the zinc binding motif was identical in the two proteins. The quality of the model was confirmed with Verify3D (Eisenberg et al., 1997). Model structures were examined using Sybyl6.8. Models of mutagens (F544V and F544I) of IRAP were constructed in PYMOL (http://www.pymol.org/) and minimized under the Tripos forcefield (Clark et al., 1989) as described above.

Conformers of the inhibitors HFI-142, HFI-419, HFI-435, and HFI-437 were created using Omega v2.3.2 and docked into the IRAP models using Fred version 2.2.5 (McGann et al., 2003). The IRAP docking box was constructed in Fred Receptor version 2.2.5 and contained an inner contour of 68 $Å^3$ and an outer contour of 1690 $Å^3$. A distance of 4 Å was added to the docking box, and the Chemgauss3 scoring function was used, which takes into account metal contacts with hydrogen bond donors and π-stacking interactions with aromatic groups (supplemental data). The top 20 poses were retained and visually analyzed in Vida (http://www.eyesopen.com) with preferred solutions chosen by a number of criteria, including the scoring

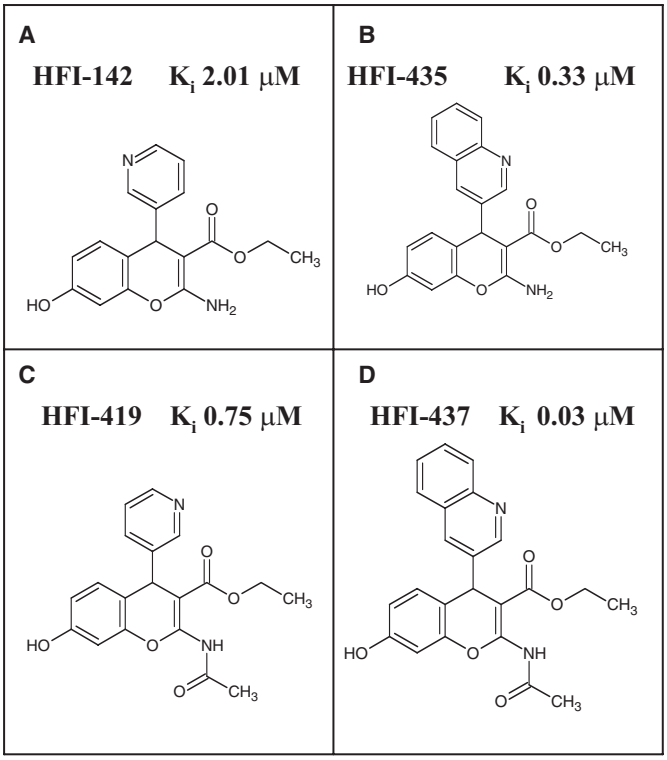

Fig. 1. Structures of the benzopyran-based IRAP inhibitors. A and C, 4-pyridinyl derivatives (HFI-142 and HFI419); B and D, 4- quinolinyl derivatives (HFI-435 and HFI-437). K_i was calculated using the synthetic substrate Leu-MCA; $K_i = IC_{50}/([S]/K_m)$, where Leu-MCA K_m = 38.7 μM and [S] = 25 μM. (Albiston et al., 2008).

function, preferred clustering of poses, and agreement with mutagenesis data.

Cell Culture and Transfection. HEK 293T cells were grown in Dulbecco's modified Eagle's medium (Trace Biosciences Pty Ltd., Sydney, NSW, Australia) supplemented with 10% heat-inactivated fetal calf serum (Trace Biosciences), 100 U/ml penicillin/streptomycin (Invitrogen, Paisley, UK), 250 U/ml amphotericin B (Fungizone; Invitrogen), and 2 mM glutamine (Trace Biosciences Pty. Ltd) at 37°C in a modified atmosphere of 95% O_2 and 5% CO_2. For transient expression, HEK 293T cells were transfected with either 20 μg of pCI-IRAP (wild-type IRAP; a gift from M. Tsujimoto, RIKEN, Saitama, Japan) or the IRAP mutants, or empty vector using Lipofectamine transfection reagent (Invitrogen) according to the manufacturer's instructions.

Site-Directed Mutagenesis. Polymerase chain reaction-based site-directed mutagenesis was carried out with the QuikChange site-directed mutagenesis kit (Stratagene, La Jolla, CA) according to the manufacturer's instructions using the full-length cDNA encoding human IRAP construct in pCI-neo vector (pCI-IRAP) as the template. DNA sequencing with an automated sequencer (371; Applied Biosystems, Foster City, CA) was used to verify mutations.

Protein Determination. Protein concentration was determined with the DC Protein Assay kit (Bio-Rad Laboratories, Hercules, CA) using bovine serum albumin as standard.

Enzymatic Activity Assay. Samples for enzyme analysis were prepared as described previously (Ye et al., 2008). The enzymatic activities of wild-type IRAP and mutants were determined by the hydrolysis of the synthetic substrate Leu-MCA monitored by the release of a fluorogenic product, MCA, at excitation and emission wavelengths of 380 and 440 nm, respectively. Assays were performed in 96-well plates; each well contained between 0.2 and 10 μg of solubilized membrane protein, a range of concentrations of substrate in a final volume of 100 μl of 50 mM Tris-HCl buffer, pH 7.4. Nonspecific hydrolysis of the substrate was corrected by subtracting the emission from incubations with membranes transfected with empty vector. Reactions were performed at 37°C for 30 min within a thermostat-equipped FLEX station fluorescence microplate reader (Molecular Devices, Sunnyvale, CA). The kinetic parameters (K_m and V) were determined by nonlinear fitting of the Michaelis-Menten equation (Prism; GraphPad Software Inc., Sna Diego, CA), using final concentrations of Leu-MCA of 15.6 μM to 1 mM. Inhibition constants (K_i) for the competitive inhibitors were calculated from the relationship $IC_{50} = K_i\ (1 + [S]/K_m)$, where IC_{50} values were determined over a range of inhibitor concentrations (10^{-9} to 10^{-4} M). The K_m values of wild-type and mutant IRAP for Leu-MCA were determined from the kinetic studies (Table 1). All data obtained were from at least three separate experiments performed in triplicate.

Determination of Substrate Degradation. The degradation of substrates by wild-type or mutant IRAP was analyzed using reversed-phase high-performance liquid chromatography as described previously (Lew et al., 2003). In brief, each peptide substrate (30 μg) was incubated at 37°C in Tris-buffered saline (100 mM Tris-HCl and 150 mM NaCl, pH 7.4) with 10 μg of solubilized membrane protein from HEK 293T cells transfected with wild-type or mutant IRAP. At each time point (0, 0.5, 1, 2, 4, and 6 h), an aliquot containing 5 μg of peptide was removed, and the reaction was stopped by addition of 4 volumes of methanol/1% trifluoroacetic acid (TFA). Samples were dried on a centrifugal vacuum evaporator (Speed-Vac; Thermo Fisher Scientific, Waltham, MA) before high-performance liquid chromatography analysis using a liquid chromatograph with on-line mass spectrometric detector (1100 series; Agilent Technologies, Palo Alto, CA). Samples were loaded onto a ZORBAX Eclipse C18 column (maintained at 50°C) in 1.8% acetonitrile, 0.1% TFA, and 0.02% acetic acid at 0.15 ml/min, and eluted with a 30-min linear gradient to 60% acetonitrile, 0.1% TFA. Fragments were identified after mass spectral analysis using Agilent ChemStation deconvolution software.

TABLE 1
Kinetic parameters for the hydrolysis of Leu-MCA by wild-type IRAP and phenylalanine-544 substituted IRAP
Data are expressed as mean ± S.E.M.

Mutants	K_m	V_{max}	V_{max}/K_m
	μM	$\mu M \cdot \mu g\ protein^{-1} \cdot h^{-1}$	$\mu g\ protein \cdot h^{-1}$
IRAP	47.1 ± 6.2	144.4 ± 5.1	3.1
[F544I]IRAP	63.7 ± 12.6	56.5 ± 3.0	0.9
[F544V]IRAP	101 ± 10.6	9.3 ± 1.1	0.1

Results

Docking of the HFI-Series Inhibitors into Wild-Type and Mutant IRAP Models

Molecular modeling of the catalytic site of IRAP based on the crystal structure of LTA4H suggested that Phe544 provides a hydrophobic packing point at one side of the active site. Computational docking of the HFI-series inhibitors (Fig. 2) suggested that this may be a key interaction for each of the inhibitors. For all four compounds, the *S*-isomer docked better, in terms of having a lower binding energy/scoring function and also a predominant and consistent binding mode in the top 20 solutions (Supplemental Data). The two pyridinyl analogs (HFI-142 and HFI-419) display a direct ring-stack interaction between the benzopyran rings and Phe544 (Fig. 2A) and orient with the Zn^{2+} ion interacting with the benzopyran oxygen and in the case of HFI-419, a second interaction with the amide carbonyl. There is also a hydrogen bond between the hydroxyl moiety and Glu295. Furthermore, numerous van der Waals interactions between compound and protein are present, particularly with residues Gln293, Pro296, Glu426, Ala427, Leu483, and Ile540 of the wild-type IRAP. The two quinolinyl analogs (HFI-435 and HFI-437) orient in a different manner. Instead of a ring stack, Phe544 contributes an edge-face hydrophobic stacking point with the benzopyran (2-amino-4-aryl-chromene) structure of the inhibitors (Fig. 2C). These inhibitors interact with the Zn^{2+} ion via the quinolinyl nitrogen. The hydroxyl moiety of the quinoline compounds hydrogen bonds to the side chains of Lys520 and Ser546. There are also numerous van der Waals contacts, particularly with Glu295, Met430, Ile461, His464, Glu494, Tyr495, and Phe550.

Docking studies of the HFI inhibitors were similarly carried out on models representing the F544V and F544I mutants. Compared with the wild-type structure, HFI-142 was able to dock in a comparable manner into the F544V mutant but adopted an alternate binding mode when docked into the F544I mutant, because the modeling predicted that the original pose is not favored because of a clash between the side chain of the isoleucine and the inhibitor. The same is true of HFI-419, but this inhibitor adopts an alternate "flipped" conformation when docked into the F544I and F544V mutants; in this pose, the 2-acetamido group of HFI-419 is available for hydrogen bonding with the side chain of Tyr549, and the Zn^{2+} interacts with the inhibitor through the benzopyran oxygen (Fig. 2B).

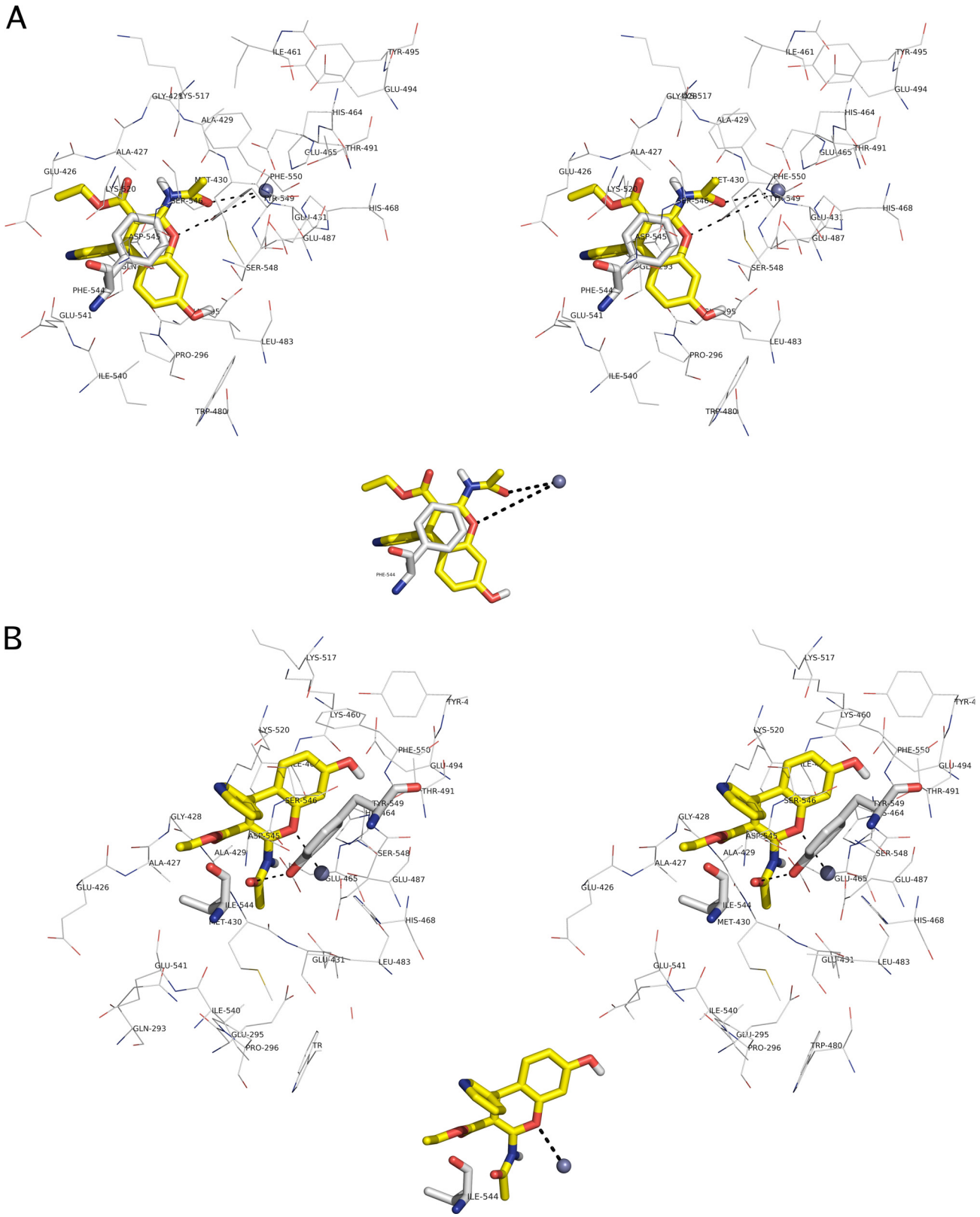

Fig. 2. Model showing the docking of HFI-419 and HFI-437 to the catalytic site. A, cross-eyed stereo view (above) and simplified view (below) of HFI-419 (yellow sticks) docked into the IRAP model. There are interactions with the Zn^{2+} ion (purple sphere) via the amide carbonyl and the benzopyran oxygen (shown as dashed lines). Phe544 (white sticks) has a direct parallel ring stacking interaction with the benzopyran. This picture is rotated 90° along the *x*-axis (see arrow) compared with the other panels in this figure. B, cross-eyed stereo (above) and simplified (below) view of mutation F544I. The mutation results in an unfavorable clash between the isoleucine side chain and the benzopyran of HFI-419 (not shown). An alternative flipped orientation is found to be prominent among the top 20 poses, which retains the Zn^{2+} interaction with the benzopyran oxygen (dashed line) and allows a hydrogen bond between the acetamide of the inhibitor and Tyr549 (dashed line). There is also an edge-face interaction between Tyr549 and the pyridinyl ring of the inhibitor.

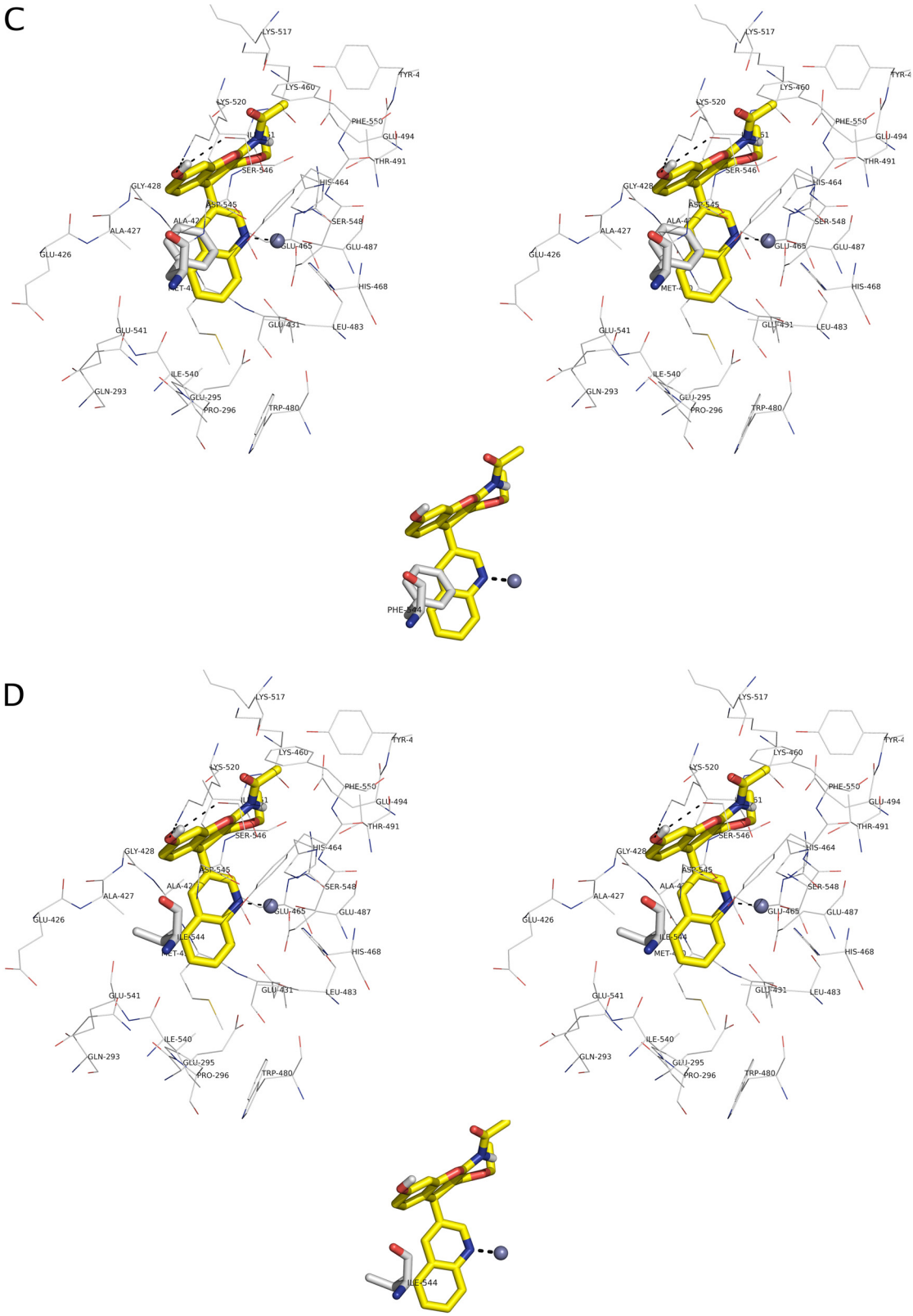

Fig. 2. *Continued.* C, cross-eyed stereo view (above) and simplified view (below) of HFI-437 (yellow sticks) docked into the IRAP model. This inhibitor has an alternate binding mode to that described for HFI-419, the quinoline nitrogen now interacting with the Zn^{2+} ion. Phe544 is an edge-face stacking point for this inhibitor. D, cross-eyed stereo (above) and simplified (below) view of the mutation F544I that would result in a loss of hydrophobic interactions with HFI-437 because the smaller side chain does not interact with the benzopyran moiety of the inhibitor. All pictures were constructed using the molecular modeling software PYMOL.

The two quinolinyl derivatives (HFI-435 and HFI-437) are oriented so that the benzopyran moiety of the inhibitors form an edge-face stacking interaction with Phe544 (Fig. 2C). While the binding pose is maintained, the side chains of these mutations do not make contact with the benzopyran moiety of the inhibitors (Fig. 2D), which is expected to result in a loss of binding affinity.

Kinetic Parameters of Recombinant Wild-Type and Mutant IRAPs

Comparative enzyme kinetic studies were conducted on wild-type and mutant IRAP (replacement of Phe544 with Ile, Val, Ala) using the synthetic substrate Leu-MCA. The turnover rate (V_{max}/K_m) obtained for the mutants correlated in part with the size and hydrophobicity of the side chain (Table 1); [F544A]IRAP demonstrated no aminopeptidase activity. The major parameter affected was the V_{max}; only modest alterations in the Michaelis constant (K_m) were observed for the other mutants (Table 1).

The ability of the mutants to metabolize the peptide substrates AVP and Leu-Enk was also investigated. The F544I mutant metabolized AVP at the same rate as the wild-type IRAP but was unable to cleave Leu-Enk (Table 2). In keeping with its low V_{max} value, the F544V mutant cleaved AVP at $<10\%$ the efficiency of the wild type and was also inactive toward Leu-Enk (Table 2). The level of perturbation of the catalytic activity of IRAP correlated with the reduction in the hydrophobic surface area and the size of the side chain of residue Phe544.

Inhibitory Potencies of Various Classes of IRAP Inhibitors

Peptide Inhibitors. Enzyme inhibition assays were carried out to investigate the effect of the mutations on the binding affinity of IRAP inhibitors. Substitution of Phe544 with either Ile or Val had no effect on the affinity of Ang IV for IRAP, whereas these mutations resulted in marked changes in the affinities both for the Ang IV analog Nle^1-Ang IV and for LVV-H7. Marked changes were observed for Nle^1-Ang IV, the affinity being 34-fold lower for the F544I mutant and 4.3-fold lower for the F544V mutant compared with wild type (Table 3). In contrast, the affinity of LVV-H7 for both mutants was approximately 2-fold lower than for wild type (Table 3). At first, Val^1 of Ang IV was substituted for Nle to stabilize the peptide for in vivo studies, presumably to reduce susceptibility to N-terminal degradation (Sardinia et al., 1994). It is interesting that in this conserved change to Nle (2-aminohexanoic acid), the unbranched isomer of leucine, the N-terminal amino acid of Ang IV has such a marked effect on binding to the mutant forms of IRAP.

HFI Series Inhibitors. Mutation of Phe544 resulted in marked changes in the affinity of some of the inhibitors for IRAP (Table 4). For the pyridinyl derivatives, only modest changes in affinities of these inhibitors for the IRAP mutants were observed, except for the affinity of HFI-142 for the F544I mutant, where nearly a 10-fold reduction in affinity was observed. In contrast, the affinities for both HFI compounds containing the quinolinyl group (HFI-435, HFI-437) were reduced by 10-fold for both the F544I and F544V mutants. The affinities were decreased to levels comparable with the affinities of the 4-pyridinyl analogs for wild-type IRAP.

TABLE 2

Degradation of AVP and Leu-Enk by wild-type and phenylalanine-544 substituted IRAP

The catalytic activity for the mutants is expressed relative to wild type (1.0).

Enzyme	Vasopressin (AVP) CYFQNCPRG	Leu-Enk YGGFL
IRAP	1.0	1.0
[F544I]IRAP	1.0	No activity
[F544V]IRAP	<0.1	No activity

Discussion

The benzopyran inhibitors of IRAP are an important new lead toward the development of therapeutics against dementia, and understanding the molecular basis of the interaction will assist progress in this field. As yet, however, the structure of IRAP has not been solved, such that models of inhibitor binding are required. We performed computational docking of some of the most active, IRAP-specific, HFI-series inhibitors (Fig. 1) onto a homology model of the catalytic domain of IRAP (based on the crystal structure of LTA4H). We were surprised to find that the docking results revealed two different binding conformations for these structurally analogous inhibitors but indicated in both cases that Phe544 would provide a hydrophobic packing point at one side of the active site.

In the binding pose adopted by the pyridinyl derivatives HFI-142 and HFI-419, a ring stack is predicted between the benzopyran moieties of the compounds and Phe544 (Fig. 2A). This binding pose contains numerous other interactions, including a hydrogen bond from the hydroxyl moiety of the inhibitors to Glu295 and van der Waals interactions involving Gln293, Pro296, Glu426, Ala427, Leu483, and Ile540. Although the binding mode of both is comparable, the higher potency of HFI-419 may be due to the added interaction with the Zn^{2+} through the amide carbonyl. HFI-142 was able to dock into the F544V mutant in a comparable manner but adopted an alternate pose when docked into the F544I mutant because of a clash with the hindered isoleucine. Consistent with this model, only a modest decrease in affinity of HFI-142 was observed for the F544V compared with wild type, whereas a much greater decrease in affinity of HFI-142 was seen for the F544I mutant IRAP (Table 4). The mutations also dramatically affected the docking of the acetamido

TABLE 3

K_i values ± S.E.M. of peptide inhibitors for phenylalanine-544 substituted IRAP

	Nle^1-Ang IV	Ang IV	LVV-H7
		μM	
IRAP	0.23 ± 0.05	0.15 ± 0.01	0.36 ± 0.04
[F544I]IRAP	7.85 ± 1.34	0.21 ± 0.03	0.72 ± 0.04
[F544V]IRAP	1.02 ± 0.33	0.18 ± 0.03	0.83 ± 0.20

Nle^1-Ang IV, NleYIHPF; Ang IV, VYIHPF; LVV-H7, LVVYPWTQRF.

TABLE 4

K_i values ± S.E.M. of HFI inhibitors for phenylalanine-544 substituted IRAP

	HFI-142	HFI-435	HFI-419	HFI-437
			μM	
IRAP	2.01 ± 0.51	0.33 ± 0.14	0.75 ± 0.30	0.031 ± 0.004
[F544I]IRAP	16.42 ± 5.22	3.72 ± 0.62	1.83 ± 0.34	0.20 ± 0.03
[F544V]IRAP	4.10 ± 0.08	2.51 ± 0.52	0.67 ± 0.13	0.27 ± 0.08

derivative HFI-419, which adopts an alternate "flipped" conformation when docked into the F544I and F544V mutants, but one that is still able to make key contacts in the binding site (Fig. 2B). That this particular inhibitor retains significant affinity in the presence of these mutations compared with the other three inhibitors (Table 4) may be explained by this alternate pose.

The quinolines (HFI-435 and HFI-437) are not able to adopt the aforementioned binding mode for the pyridinyl compounds because the large quinoline group is too large to enter the small polar pocket formed by Glu426 and Glu293. Alternatively, they adopt a mode that allows a stronger interaction with the zinc atom through the quinoline nitrogen. The quinoline compounds are predicted to be more active than the pyridinyl compounds because of the more favorable coordination with the zinc atom, along with the hydrogen bonding network between the hydroxyl moiety of the inhibitors and Ser546 and Lys520 and better van der Waals contacts, particularly the quinoline ring with the side chain of Met430 and the ethyl ester with Ile461. The addition of an acetyl group to the amino of HFI-435 fills a space and results in HFI-437 having additional contacts with Phe550 and Tyr495, perhaps accounting for its greater potency.

The significant decline in affinity of HFI-435 and HFI-437 seen with both mutations F544V/I is likely to be a direct result of a loss of the edge-face hydrophobic interactions between Phe544 and the benzopyran (Fig. 2C). In the docking of these inhibitors into the mutant forms, the binding pose is maintained as the strong interaction with the zinc atom is not hindered by the mutations as with the pyridinyl compounds. However, the smaller side chains of these mutations do not make contact with the benzopyran moiety of the inhibitors (Fig. 2D).

From a medicinal chemistry perspective, these results are potentially very important, because they indicate that IRAP is capable of binding these benzopyran inhibitors in multiple alternate orientations, and this provides for multiple options in the elaboration of the ligands to improve their pharmaceutical properties. In essence, the enzyme is seeing not one chemical class but two (and possibly three), and the pyridinyl series and quinolinyl series would be expected to display different structure-activity relationships. Our preliminary medicinal chemistry campaign to some extent supports this concept.

As well as the effects on the HFI series, the variable importance of Phe544 in defining the IRAP catalytic site is reflected in the results obtained for peptide substrate cleavage. Neither mutant was able to cleave Leu-Enk, suggesting that a ring stack interaction of the amino-terminal tyrosine residue of Leu-Enk with Phe544 may be essential for the correct orientation of the substrate in the catalytic site. In contrast, AVP cleavage by the mutants correlated well with the V_{max} of the mutants, indicating that Phe544 does not play a pivotal role in the orientation of AVP in the catalytic site. In keeping with these data is the model for binding of an arginyl tripeptide substrate to LTA4H. In this model, Tyr378, the residue corresponding to Phe544 in IRAP, plays a role in defining the S1 and S2′ subsites of the active site (Thunnissen et al., 2002).

The inhibitory properties of the peptide inhibitors were unaffected by the mutation of Phe544 except for Nle^1-Ang IV inhibition of the F544I mutant IRAP. These results suggest that the Phe544 hydrophobic stacking point does not make a significant contribution to the binding affinities of the peptide inhibitors for IRAP. The 30-fold lower affinity of Nle^1-Ang IV for the F544I IRAP compared with wild type is predicted to be due to the side chain of the isoleucine clashing with Nle; this is comparable with the interaction of the pyridinyl inhibitors with the isoleucine side chain predicted by the in silico modeling (Fig. 1).

The aromatic R group residue, represented by Phe544 in IRAP, is conserved throughout the M1 family, the corresponding residue being either a Phe or a Tyr. The importance of the Phe544 in the catalytic site of IRAP is consistent with insights obtained from studies on the crystal structures of a number of M1 aminopeptidases, including human LTA4H (Thunnissen et al., 2001), bacterial APN (Ito et al., 2006), and plasmodium M1 alanyl aminopeptidase (*Pf*A-M1) (McGowan et al., 2009). These structures were resolved with the nonspecific aminopeptidase inhibitor bestatin, an analog of the dipeptide Phe-Leu, present in the active site. In each case, the phenolic ring of bestatin is demonstrated to be important in stabilizing the binding of bestatin in the catalytic site of these M1 aminopeptidases. In the crystal structure of bacterial APN, Tyr376, the equivalent amino acid residue, forms a hydrophobic stacking with the phenyl ring of bestatin in the active site (Ito et al., 2006; Addlagatta et al., 2008). The importance of this amino acid residue extends to its interactions with inhibitors of other aminopeptidases; for example, the LTA4H competitive thioamine inhibitor 3-(4-benzyloxyphenoyl)-2-(*R*)-amino-1-propane thiol was shown to bind to the zinc and the hydrophobic pocket with the proximal phenyl ring, making stacking interactions with Tyr378 (Phe544 equivalent) and Tyr267 (Thunnissen et al., 2001, 2002). Moreover Tyr378 in LTA4H also plays a critical role in suicide inactivation of LTA4H epoxide hydrolase activity (Mueller et al., 1996a,b).

In conclusion, we have demonstrated the involvement of Phe544 in defining the interaction of two classes of benzopyran derived IRAP inhibitors with its catalytic site, which is reflected in the altered potencies in binding to wild-type and conserved Phe544 mutant IRAP. The docking studies suggest that for the pyridinyl HFI inhibitors, the benzopyran moiety interacts in a ring stack with Phe544. In contrast, the docking studies led to the hypothesis that because of the different orientation of the quinolinyl HFI inhibitors in the catalytic site, Phe544 provides an edge-face hydrophobic stacking point with the benzopyran. Moreover, we demonstrated that Phe544 does not play a pivotal role in determining the potencies of the peptide inhibitors. These new insights into the orientation of the HFI inhibitors in the IRAP catalytic site provide key information for pharmacophore design for IRAP inhibitors, paving the way for the development of a new generation of IRAP inhibitors for use as central-acting memory enhancing agents.

References

Addlagatta A, Gay L, and Matthews BW (2008) Structural basis for the unusual specificity of Escherichia coli aminopeptidase N. *Biochemistry* **47:**5303–5311.

Albiston AL, Morton CJ, Ng HL, Pham V, Yeatman HR, Ye S, Fernando RN, De Bundel D, Ascher DB, Mendelsohn FA, et al. (2008) Identification and characterization of a new cognitive enhancer based on inhibition of insulin-regulated aminopeptidase. *FASEB J* **22:**4209–4217.

Albiston AL, Pederson ES, Burns P, Purcell B, Wright JW, Harding JW, Mendelsohn FA, Weisinger RS, and Chai SY (2004a) Reversal of scopolamine-induced memory deficits by LVV-hemorphin 7 in rats in the passive avoidance and Morris water maze paradigms. *Behav Brain Res* **154:**239–243.

Albiston AL, Ye S, and Chai SY (2004b) Membrane bound members of the M1 family: more than aminopeptidases. *Protein Pept Lett* **11:**491–500.

Andersson H, Demaegdt H, Vauquelin G, Lindeberg G, Karlén A, and Hallberg M (2008) Ligands to the (IRAP)/AT4 receptor encompassing a 4-hydroxydiphenylmethane scaffold replacing Tyr2. *Bioorg Med Chem* **16:**6924–6935.

Axén A, Andersson H, Lindeberg G, Rönnholm H, Kortesmaa J, Demaegdt H, Vauquelin G, Karlén A, and Hallberg M (2007) Small potent ligands to the insulin-regulated aminopeptidase (IRAP)/AT(4) receptor. *J Pept Sci* **13:**434–444.

Clark M, Cramer RD, and Van Opdenbosch N (1989) Validation of the general purpose Tripos 5.2 force field. *J Comput Chem* **10:**982–1012.

Demaegdt H, Lenaerts PJ, Swales J, De Backer JP, Laeremans H, Le MT, Kersemans K, Vogel LK, Michotte Y, Vanderheyden P, and Vauquelin G (2006) Angiotensin AT4 receptor ligand interaction with cystinyl aminopeptidase and aminopeptidase N: [^{125}I]angiotensin IV only binds to the cystinyl aminopeptidase apoenzyme. *Eur J Pharmacol* **546:**19–27.

Eisenberg D, Lüthy R, and Bowie JU (1997) VERIFY3D: assessment of protein models with three-dimensional profiles. *Methods Enzymol* **277:**396–404.

Herbst JJ, Ross SA, Scott HM, Bobin SA, Morris NJ, Lienhard GE, and Keller SR (1997) Insulin stimulates cell surface aminopeptidase activity toward vasopressin in adipocytes. *Am J Physiol* **272:**E600–E606.

Ito K, Nakajima Y, Onohara Y, Takeo M, Nakashima K, Matsubara F, Ito T, and Yoshimoto T (2006) Crystal structure of aminopeptidase N (proteobacteria alanyl aminopeptidase) from Escherichia coli and conformational change of methionine 260 involved in substrate recognition. *J Biol Chem* **281:**33664–33676.

Krishnan R, Hanesworth JM, Wright JW, and Harding JW (1999) Structure-binding studies of the adrenal AT4 receptor: analysis of position two- and three-modified angiotensin IV analogs. *Peptides* **20:**915–920.

Lee J, Albiston AL, Allen AM, Mendelsohn FA, Ping SE, Barrett GL, Murphy M, Morris MJ, McDowall SG, and Chai SY (2004) Effect of intracerebroventricular injection of AT4 receptor ligands, Nle1-angiotensin IV and LVv-hemorphin 7, on spatial learning in rats. *Neuroscience* **124:**341–349.

Lee JH, Mustafa T, McDowall SG, Mendelsohn FAO, Brennan MB, Lew R, Albiston AL, and Chai SY (2003) Structure-activity study of LVV-hemorphin-7: angiotensin AT4 receptor ligand and inhibitor of insulin-regulated aminopeptidase (IRAP). *J Pharmacol Exp Ther* **305:**205–211.

Lew RA, Mustafa T, Ye S, McDowall SG, Chai SY, and Albiston AL (2003) Angiotensin AT4 ligands are potent, competitive inhibitors of insulin regulated aminopeptidase (IRAP). *J Neurochem* **86:**344–350.

Lukaszuk A, Demaegdt H, Feytens D, Vanderheyden P, Vauquelin G, and Tourwé D (2009) The replacement of His(4) in angiotensin IV by conformationally constrained residues provides highly potent and selective analogues. *J Med Chem* **52:**5612–5618.

Lukaszuk A, Demaegdt H, Szemenyei E, Tóth G, Tymecka D, Misicka A, Karoyan P, Vanderheyden P, Vauquelin G, and Tourwé D (2008) Beta-homo-amino acid scan of angiotensin IV. *J Med Chem* **51:**2291–2296.

McGann MR, Almond HR, Nicholls A, Grant JA, and Brown FK (2003) Gaussian Docking Functions. *Biopolymers* **68:**76–90.

McGowan S, Porter CJ, Lowther J, Stack CM, Golding SJ, Skinner-Adams TS, Trenholme KR, Teuscher F, Donnelly SM, Grembecka J, et al. (2009) Structural basis for the inhibition of the essential Plasmodium falciparum M1 neutral aminopeptidase. *Proc Natl Acad Sci USA* **106:**2537–2542.

Mueller MJ, Andberg MB, Samuelsson B, and Haeggström JZ (1996a) Leukotriene A4 hydrolase, mutation of tyrosine 378 allows conversion of leukotriene A4 into an isomer of leukotriene B4. *J Biol Chem* **271:**24345–24348.

Mueller MJ, Blomster M, Oppermann UC, Jörnvall H, Samuelsson B, and Haeggström JZ (1996b) Leukotriene A4 hydrolase: protection from mechanism-based inactivation by mutation of tyrosine-378. *Proc Natl Acad Sci USA* **93:**5931–5935.

Olson ML, Olson EA, Qualls JH, Stratton JJ, Harding JW, and Wright JW (2004) Norleucine1-angiotensin IV alleviates mecamylamine-induced spatial memory deficits. *Peptides* **25:**233–241.

Pederson ES, Harding JW, and Wright JW (1998) Attenuation of scopolamine-induced spatial learning impairments by an angiotensin IV analog. *Regul Pept* **74:**97–103.

Pederson ES, Krishnan R, Harding JW, and Wright JW (2001) A role for the angiotensin AT4 receptor subtype in overcoming scopolamine-induced spatial memory deficits. *Regul Pept* **102:**147–156.

Sardinia MF, Hanesworth JM, Krebs LT, and Harding JW (1993) AT4 receptor binding characteristics: D-amino acid- and glycine- substituted peptides. *Peptides* **14:**949–954.

Sardinia MF, Hanesworth JM, Krishnan F, and Harding JW (1994) AT4 receptor structure-binding relationship: N-terminal-modified angiotensin IV analogues. *Peptides* **15:**1399–1406.

Saveanu L, Carroll O, Weimershaus M, Guermonprez P, Firat E, Lindo V, Greer F, Davoust J, Kratzer R, Keller SR, et al. (2009) IRAP identifies an endosomal compartment required for MHC class I cross-presentation. *Science* **325:**213–217.

Segura E, Albiston AL, Wicks IP, Chai SY, and Villadangos JA (2009) Different cross-presentation pathways in steady-state and inflammatory dendritic cells. *Proc Natl Acad Sci USA* **106:**20377–20381.

Stragier B, Clinckers R, Meurs A, De Bundel D, Sarre S, Ebinger G, Michotte Y, and Smolders I (2006) Involvement of the somatostatin-2 receptor in the anticonvulsant effect of angiotensin IV against pilocarpine-induced limbic seizures in rats. *J Neurochem* **98:**1100–1113.

Thunnissen MM, Nordlund P, and Haeggström JZ (2001) Crystal structure of human leukotriene A(4) hydrolase, a bifunctional enzyme in inflammation. *Nat Struct Biol* **8:**131–135.

Thunnissen MM, Andersson B, Samuelsson B, Wong CH, and Haeggström JZ (2002) Crystal structures of leukotriene A4 hydrolase in complex with captopril and two competitive tight-binding inhibitors. *FASEB J* **16:**1648–1650.

Wiśniewski K, Borawska M, and Car H (1993) The effect of angiotensin II and its fragments on post-alcohol impairment of learning and memory. *Pol J Pharmacol* **45:**23–29.

Ye S, Chai SY, Lew RA, Ascher DB, Morton CJ, Parker MW, and Albiston AL (2008) Identification of modulating residues defining the catalytic cleft of insulin-regulated aminopeptidase. *Biochem Cell Biol* **86:**251–261.

Address correspondence to: Siew Yeen Chai, Howard Florey Institute, University of Melbourne, Parkville, Victoria 3010, Australia. E-mail: sychai@florey.edu.au